arXiv:1603.08956v1 [astro-ph.SR] 29 Mar 2016

Simulating radially outward winds within a turbulent gas clump

Guillermo Arreaga-García[1] and Silvio Oreste Topa[2]

[1] Departamento de Investigación en Física
Universidad de Sonora
Hermosillo, Sonora, MEXICO
garreaga@cifus.uson.mx
[2] EESA Num. 1,
Tornquist, Pcia. de Buenos Aires
ARGENTINA

Abstract. By using the particle-based code Gadget2, we follow the evolution of a gas clump, in which a gravitational collapse is initially induced. The particles representing the gas clump have initially a velocity according to a turbulent spectrum built in a Fourier space of 64^3 grid elements. In a very early stage of evolution of the clump, a set of gas particles representing the wind, suddenly move outwards from the clump's center. We consider only two kinds of winds, namely: one with spherical symmetry and a second one being a bipolar collimated jet. In order to assess the dynamical change in the clump due to interaction with the winds, we show iso-velocity and iso-density plots for all our simulations.

Keywords: winds,turbulence,collapse,hydrodynamics,simulations

1 Introduction

Stars are born in large gas structures made of molecular hydrogen. These gas structures are named clumps; see Ref. [1]. These clumps have typical sizes and masses of a few pc (parsecs) and a few hundred or even thousands of $M_\odot$ (one solar mass), respectively[3].

The physical process by which the molecular gas is transformed from a gas structure into some stars is mainly gravitational collapse, whose main effects on the gas clump are that the gas density is increased while its size is reduced. At some point during this transformation process from gas to star, the densest gas structures settled down in more or less dynamically stable gas objects called protostars[4]. For instance, the number density of a typical large clump structure ranges around 10^3 molecules per cm^{-3} whilst that of a typical protostar ranges around 10^{14} molecules per cm^{-3}. To achieve a better understanding of the huge change in scales, we mention that the number density of a typical star is around 10^{24} molecules per cm^{-3}. The results of a set of numerical simulations aimed to study the gravitational collapse of a spherically symmetric, rigidly rotating, isolated, interstellar gas core are presented in Ref. [2].

The process of gravitational collapse is not the only process acting upon the gas structures in the interstellar medium, as many other phenomena can have a great influence on the evolution of the clump, among others: (i) the highly ionized gas ejected by the explosion of supernovas; (ii) the

[3] A parsec (pc) is equivalent to 3.08×10^{18} cm and a solar mass $M_\odot$ is equivalent to 1.99×10^{33} g.

[4] Any star does radiate its own energy produced by thermonuclear reactions in its interior, but a protostar does not. This is the main difference between a star and a protostar; but they can share some dynamical properties as they are stable structures of different stages of the same formation process.

bipolar collimated winds ejected by a massive protostar; (iii) rapidly expanding H_{II} regions which hit the slower and less dense gas structures.

Recently, in Ref.[3], a set of SPH simulations were conducted to study star formation triggered by an expanding H_{II} region within a spherical gas structure with uniform density that was not globally collapsing. The expanding shock plays the role of a snowplow, which sweeps out the gas of the surrounding medium. The density of the swept out gas increases as a consequence of this agglomeration process, and a gravitational collapse may then be locally initiated. Small gas over-densities can be formed in this way, which may achieve the protostar stage. Because these two processes are complementary in forming proto-stars, this star formation scenario was named the collect and collapse model.

Furthermore, in order to study the effects of proto-stellar outflows on the turbulence of a star forming region, in Refs.[4] and [5], magneto-hydrodynamics simulations (MHD) were conducted with a mesh based code which implements the Adaptive Mesh Refinement technique (AMR).

In this paper, we investigate the change in the dynamical configuration of a typical turbulent clump when a wind of particles is outwardly ejected from the central region of the clump. The most important difference between the present paper and Ref. [3] is the turbulent nature of our clump. Turbulence makes a big change in the spatial distribution as the clump becomes filamentary and flocculent.

2 The physical system

In this section we briefly describe the physics of the clump and the winds, which will be considered in the following sections.

2.1 The initial clump

We here consider a typical spherical clump with a radius $R_0 = 2$ pc and mass $M_0 = 1219\, M_\odot$. Initially, it has a radially uniform density distribution with an average density given by $\rho_0 = 2.4 \times 10^{-21}$ g cm^{-3}, which is equivalent to a number density $n_0 \approx 600$ molecules cm^{-3} for molecular hydrogen with molecular mass $\mu = 4.0 \times 10^{-24}$ gr/mol. The size and mass of this clump are chosen here to be typical in the statistical sense, in accordance with Ref. [1].

The free fall time t_{ff} is defined as the time needed for an external particle to reach the center of the clump when gravity is the only force pulling the particle. In this idealized gravitational collapse, we have

$$t_{ff} \approx \sqrt{\frac{3\,\pi}{32\,G\,\rho_0}} \tag{1}$$

where G is Newton's universal gravitational constant. For our clump, we have $t_{ff} = 1.3 \times 10^6$ years.

Following Ref. [6], the dynamical properties of the initial distribution of the gas are usually characterized by α, the ratio of the thermal energy to the gravitational energy, and β, that of the rotational energy to the gravitational energy. For a spherical clump, the approximate total gravitational potential energy is $< E_{grav} > \approx -\frac{3}{5}\,\frac{G\,M_0^2}{R_0}$. The average total thermal energy $< E_{therm} >$ (kinetic plus potential interaction terms of the molecules) is $< E_{therm} > \approx \frac{3}{2}\mathcal{N}\,k\,T = \frac{3}{2}M_0\,c_0^2$, where k is the Boltzmann constant, T is the equilibrium temperature, $\mathcal{N}$ is the total number of molecules in the gas and c_0 is the speed of sound, see Section 3.4 for a more precise definition.

The kinetic energy $< E_{kin} >$ can be estimated by $M_0\, v_{av}^2/2$, where v_{av} is the average translational velocity of the clump. In order to have both energies of the same order of magnitude, $< E_{kin} > \approx < E_{grav} >$, the gas elements of the clump must attain average velocities within the range

$$v_{av}/c_0 \approx 3 - 3.5 \tag{2}$$

or $v_{av} \approx 1.6\,\mathrm{km/s}$, for a speed of sound given by

$$c_0 = 0.54\,\mathrm{km/s} \equiv 54862.91\,\mathrm{cm/s} \tag{3}$$

so that the corresponding temperature associated with the clump is $T \approx 25\,\mathrm{K}$.

It is possible to define the crossing time by means of

$$t_{cr} \approx \frac{R_0}{c_0} = 3.56 \times 10^6\,\mathrm{yr} \tag{4}$$

which sets a time scale for a sound wave to travel across the clump. To make the crossing time comparable in magnitude to the free fall time of Eq. 1, the front wave must have velocities around $v_{req}/c_0 \approx 2.6$ or $v_{req} \approx 1.45$ km/s, which are velocities a little bit slower than the ones estimated above, see Eq. 2. Anyway, in this paper we will treat propagation velocities of gas particles ranging around $2 - 3$ Mach.

2.2 The wind.

In this paper we consider two kinds of winds: the first kind has a fully spherical symmetry and the second kind is a bipolar collimated jet.

The dynamical characteristics of the wind strongly depends on its type of source. All stars eject winds of the first kind, which are driven by the stellar radiation. For instance, in cool stars, like the ones observed in the AGB (asymtotic giant branch) of the Galaxy, the winds cause a mass loss in the range $10^{-8} - 10^{-4}\,M_\odot/\mathrm{yr}$ whereas the terminal wind velocities are around $10 - 45\,\mathrm{km/s}$. In OB stars, the mass loss ranges over $10^{-6} - 10^{-4}\,M_\odot/\mathrm{yr}$ and the terminal wind velocities can go up to thousands of km/sec.

Supernovas dump around 10^4 joules of thermal and kinetic energy into the interstellar medium. But there are many types of supernovas, so that the mass losses and terminal velocities are very different, see Ref. [7]. For example, for a supernova whose progenitor was a He star, the mass loss and terminal velocities are within the ranges $10^{-7} - 10^{-4}\,M_\odot/\mathrm{yr}$ and $100 - 1000$ km/sec, respectively. When the progenitor was a RSG star, then their values ranges over $10^{-5} - 10^{-4}\,M_\odot/\mathrm{yr}$ and $10 - 40$ km/s, respectively.

It seems that all protostars eject highly collimated jets of gas during their formation process by gravitational collapse. The origin of these jets is still unclear but it may be that the accretion disk and magnetic field around the protostars play a crucial role in determining the velocities and the degree of collimation of the jets. For the molecular winds associated with protostarts of Class 0 and Class 1, the characteristic velocities are around 20 km/sec. However, for optical jets of highly ionized gas, the typical jet velocities are a few hundred km/sec. See Ref. [8] and the references therein.

3 The Computational Method

In this section we briefly describe the way we set up the physical system outlined above in computational terms.

3.1 The initial configuration of particles.

We set $N = 10$ million SPH particles for representing the gas clump. By means of a rectangular mesh we make the partition of the simulation volume in small elements each with a volume $\Delta x\,\Delta y\,\Delta z$; at the center of each volume we place a particle (the ith, say), with a mass determined by its location according to the density profile being considered, that is: $m_i = \rho(x_i, y_i, z_i) * \Delta x\,\Delta y\,\Delta z$ with $i = 1, ..., N$. Next, we displace each particle from its location by a distance on the order of $\Delta x/4.0$ in a random spatial direction.

As was stated earlier, in this paper we only consider a uniform density clump, for which $\rho(x_i, y_i, z_i) \equiv \rho_0$, for all the simulations (see Section 2.1). Therefore, all the particles have the same mass irrespective of whether a wind or clump particle.

3.2 The initial turbulent velocity of particles.

To generate the turbulent velocity spectrum for the clump particles, we follow a procedure based on the papers [9] and [10]. We set a second mesh N_x, N_y, N_z with the size of each element given by $\delta x = R_0/N_x$, $\delta y = R_0/N_y$ and $\delta z = R_0/N_z$. In Fourier space, the partition is $\delta K_x = 1.0/\left(N_x \times \delta x\right)$, $\delta K_y = 1.0/\left(N_y \times \delta y\right)$ and $\delta K_z = 1.0/\left(N_z \times \delta z\right)$. Each Fourier mode has the components $K_x = i_{K_x}\delta K_x$, $K_y = i_{K_y}\delta K_y$ and $K_z = i_{K_z}\delta K_z$, where the indices i_{K_x}, i_{K_y} e i_{K_z} take values in $[-N_x/2, N_x/2]$, $[-N_y/2, N_y/2]$ and $[-N_z/2, N_z/2]$, respectively. The wave number magnitude is $K = \sqrt{K_x^2 + K_y^2 + K_z^2}$, and so $K_{min} = 0$ and $K_{max} = \frac{\sqrt{3}\,N_x}{2\,R_0}$. The Fourier wave can equally be described by a wave length $\lambda = 2\,\pi/K$, then we see that $K \approx \frac{1}{R_0}$ and $\lambda \approx R_0$.

Following [10], the components of the particle velocity are

$$\boldsymbol{v} = \Sigma_{-K_{max}}^{K_{max}} \left| K^{\frac{-n-2}{2}} \right| \times \begin{cases} \left[K_z\, C_{K_y} \sin\left(\boldsymbol{K}\cdot\boldsymbol{r} + \Phi_{K_y}\right) - K_y\, C_{K_z} \sin\left(\boldsymbol{K}\cdot\boldsymbol{r} + \Phi_{K_z}\right)\right] \text{for } v_x \\ \left[-K_x\, C_{K_z} \sin\left(\boldsymbol{K}\cdot\boldsymbol{r} + \Phi_{K_z}\right) + K_z\, C_{K_x} \sin\left(\boldsymbol{K}\cdot\boldsymbol{r} + \Phi_{K_x}\right)\right] \text{for } v_y \\ \left[-K_x\, C_{K_y} \sin\left(\boldsymbol{K}\cdot\boldsymbol{r} + \Phi_{K_y}\right) + K_y\, C_{K_x} \sin\left(\boldsymbol{K}\cdot\boldsymbol{r} + \Phi_{K_x}\right)\right] \text{for } v_z \end{cases} \tag{5}$$

where the spectral index n was fixed at $n = -1$ and thus we have $v^2 \approx K^{-3}$. The vector $\boldsymbol{C}_K$ whose components are denoted by $\left(C_{K_x}, C_{K_y}, C_{K_z}\right)$, take values obeying a Rayleigh distribution. The wave phase vector, Φ_K, given by $\left(\Phi_{K_x}, \Phi_{K_y}, \Phi_{K_z}\right)$ takes random values on the interval $[0, 2\,\pi]$. The components of the vector $\boldsymbol{C}$ are calculated by means of $C = \sigma \times \sqrt{-2.0 \times \log\left(1.0 - u\right)}$, where u is a random number in $(0, 1)$. σ is a fixed parameter with value $\sigma = 1.0$.

3.3 The set up of the particle wind.

Let us consider the equation of mass conservation for a set of particles moving radially outwards, that is

$$\dot{M} = 4\,\pi\,r^2\,\rho(r) \times v(r) \tag{6}$$

We fix the mass loss $\dot{M}$ as a parameter of the simulation and also fix the wind density to have the uniform value ρ_0. We then determine the wind velocities according to Eq. 6. As the velocity magnitude diverges for particles around $r \approx 0$, we set a cut velocity value such that the maximum velocity allowed in our simulations is v_{max}.

Of course, there are other possibilities, which will be considered elsewhere: one is to fix the radial density $\rho(r)$ and/or the velocity profile $v(r)$ in order to obtain the mass loss $\dot{M}$ as a result.

Besides, for modeling an expanding H_{II} region, the authors of Ref. [3] proposed another and more complicated velocity function, but anyway it gives a constant expansion velocity at the last stages of time evolution, so that the average velocity of the shocked shell considered by [3] is $v_{cc}/c_0 \approx 5.6$ or $v_{cc} \approx 3.7$ km/s.

3.4 Initial energies

In a particle based code, we approximate the thermal energy of the clump by calculating the sum over all the N particles described in Section 3.1, that is

$$E_{therm} = \sum_{i=1}^{N} \frac{3}{2} \frac{P_i(\rho)\, m_i}{\rho_i}\,, \tag{7}$$

where P_i is the pressure associated with particle i with density ρ_i by means of the equation of state given in Eq. 12. In a similar way, the approximate potential energy is

$$E_{pot} = \sum_{i=1}^{N} \frac{1}{2}\, m_i\, \Phi_i\,. \tag{8}$$

where Φ_i is the gravitational potential of particle i. For the clump considered in this paper, the values of the speed of sound c_0 (see Eq. 3) and the level of turbulence are chosen so that the energy ratios have the numerical values

$$\begin{aligned} \alpha &\equiv \tfrac{E_{therm}}{|E_{grav}|} = 0.3 \\ \beta &\equiv \tfrac{E_{kin}}{|E_{grav}|} = 1.0 \end{aligned} \tag{9}$$

3.5 Resolution and thermodynamical considerations

Following Refs. [11] and [12], in order to avoid artificial fragmentation, the SPH code must fulfil certain resolution criteria, imposed on the Jeans wavelength λ_J, which is given by

$$\lambda_J = \sqrt{\frac{\pi\, c^2}{G\, \rho}}\,, \tag{10}$$

where c is the instantaneous speed of sound and ρ is the local density. To obtain a more useful form for a particle based code, the Jeans wavelength λ_J is transformed into the Jeans mass given by

$$M_J \equiv \frac{4}{3}\pi\, \rho \left(\frac{\lambda_J}{2}\right)^3 = \frac{\pi^{\frac{5}{2}}}{6} \frac{c^3}{\sqrt{G^3\, \rho}}\,. \tag{11}$$

In this paper, the values of the density and speed of sound are updated according to the following equation of state

$$p = c_0^2\, \rho \left[1 + \left(\frac{\rho}{\rho_{crit}}\right)^{\gamma - 1}\right], \tag{12}$$

as proposed by [13], where $\gamma \equiv 5/3$ and for the critical density we assume the value $\rho_{crit} = 5.0{\times}10^{-14}$ g cm^{-3}.

For the turbulent clump under consideration, we have $m_r \approx M_J/(2N_{neigh}) \approx 7.47 \times 10^{33}$ g, where we take $N_{neigh} = 40$.

In this paper, the mass of an SPH particle is $m_p = 1.98 \times 10^{29}$ g, so that $m_p/m_r = 2.5 \times 10^{-4}$ and therefore the Jeans resolution requirement is satisfied very easily.

In a previous paper of collapse reported in Ref.[14], by means of a convergence study, we demonstrated the correctness of a regular cartesian grid to make collapse calculation, as is used here to make the partition of the simulation domain in small volume elements, each of which has a SPH particle located not necessarily in its center, see Sect.3.1.

4 The evolution code

We carry out the time evolution of the initial distribution of particles with the fully parallel Gadget2 code, which is described in detail by Ref.[15]. Gadget2 is based on the $tree - PM$ method for computing the gravitational forces and on the standard SPH method for solving the Euler equations of hydrodynamics. *Gadget*2 incorporates the following standard features: (i) each particle i has its own smoothing length h_i; (ii) the particles are also allowed to have individual gravitational softening lengths ϵ_i, whose values are adjusted such that for every time step $\epsilon_i\, h_i$ is of order unity. Gadget2 fixes the value of ϵ_i for each time-step using the minimum value of the smoothing length of all particles, that is, if $h_{min} = min(h_i)$ for $i = 1, 2...N$, then $\epsilon_i = h_{min}$.

The *Gadget*2 code has an implementation of a Monaghan-Balsara form for the artificial viscosity, see Ref.[16] and Ref.[17]. The strength of the viscosity is regulated by setting the parameter $\alpha_\nu = 0.75$ and $\beta_\nu = \frac{3}{2} \times \alpha_\nu$, see Equation (14) in Ref.[15]. We here fix the Courant factor to 0.1.

We now mention here that the public Gadget2 code used in this paper, presents some potential technical problems when wind particles are simultaneously evolved with clump particles; these problems are caused by the different mass scales involved, as the discretized version of the Navier-Stokes hydrodynamical equations are written in the so called density-entropy formulation, see Ref.[18]: mainly that the particle time-step becomes prohibitively small to achieve the overall evolution of the system.

We finally mention that the initial condition code was written in ANSI-C and it makes use of a Fourier mesh of 643 grid elements in order to obtain the turbulent velocity field of 10 million SPH particles. It takes 300 CPU hours running on one INTEL-Xeon processor at 3.2 GHz. All the simulations presented in this work were conducted on a high performance Linux cluster with 46 dual cores located at the University of Sonora (ACARUS). The simulations were calculated over 300 CPU hours on a fully parallelized scheme using 12 cores per each run. The proprietary program pvwave-8.0 was used as the main the visualization tool for showing the results of this paper.

5 Results

To present the results of our simulations, we consider a slice of particles around the equatorial plane of the clump; with these particles (around 10,000) we make plots containing two complementary panels: one to show colored regions of iso-density and the other one to show the velocity field of the particles. We also make $3D$ plots built with the 500,000 densest particles of each simulation. Later, we present plots with the velocity distributions and radial velocity profile, for which we use all the simulation particles.

In Table 1 we show the values we use to define the simulations and also we give some results described below. In this Table and in all the subsequent figures, we use the following labels: "Tur" to indicate the gas clump; when the winds appear within the clump, we use the label "Tur+Wind" to refer to the spherically symmetric case and the label "Tur+Wind+Col" for the bipolar jet.

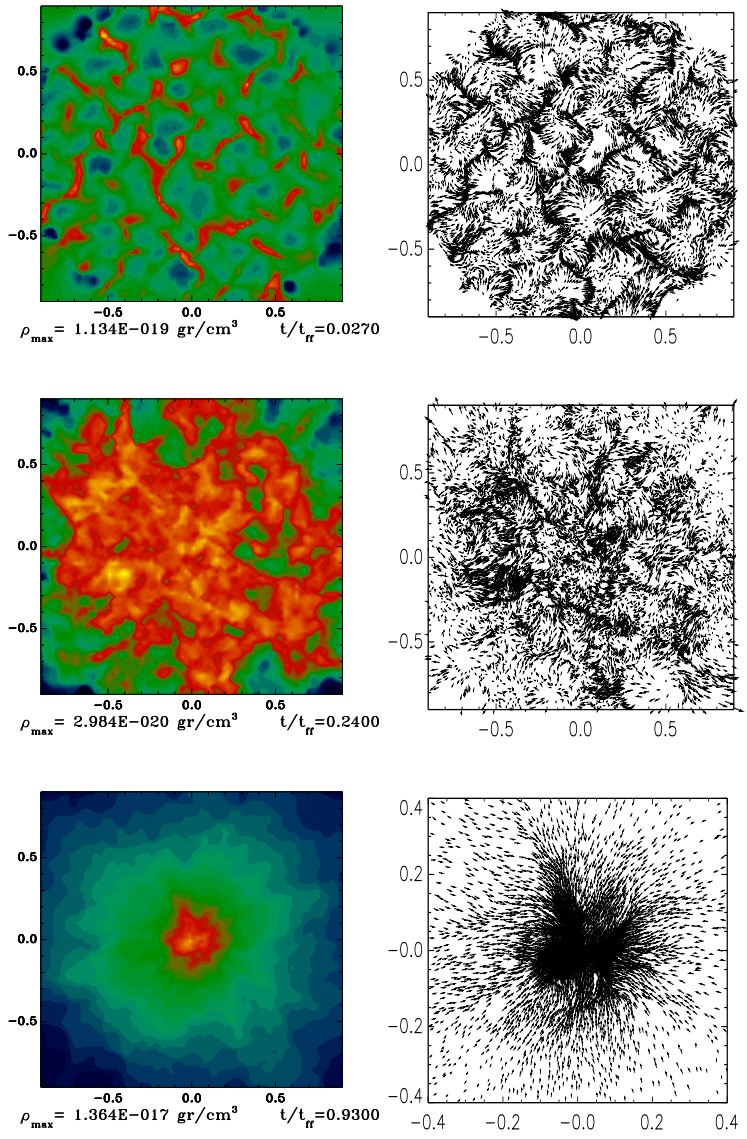

Fig. 1. Iso-density plots for the turbulent clump.

Table 1. The models.

Label	t_{start}/t_{ff}	$\dot{M}$ $[M_\odot/\mathrm{yr}]$	$\frac{R_s}{R_0}$	M_g $[M_\odot]$	M_∞ $[M_\odot]$	v_{max}/c_s	v_∞/c_s
T	0.0	—	—	1219	333	100	10
Tur+Wind	0.05	1.0×10^{-4}	0.1	6.84	359	100	11
Tur+Wind+Col	0.05	1.0×10^{-3}	0.05	4.51	422	100	72

5.1 The evolution of the turbulent clump.

One of the characteristics of turbulence is the appearance of a filamentary and flocculent structure across the clump, a structure which can already be seen in the first two panels of Fig.1. Because of the initial conditions chosen for the clump, there is a clear tendency to a global collapse towards its central region, as can be seen in the last panels of Fig.1.

We emphasize now a very important fact occurring at the outer regions of the turbulent clump. The turbulent clump is not in hydrodynamic equilibrium and there is no external pressure acting upon the clump, then the outermost particles have a non equilibrated thermal pressure. Therefore, the outer clump particles expand outwards. So, we have to keep in mind this expansion effect for the problem at hand, as we shall quantify the mass of the clump swept out by the winds.

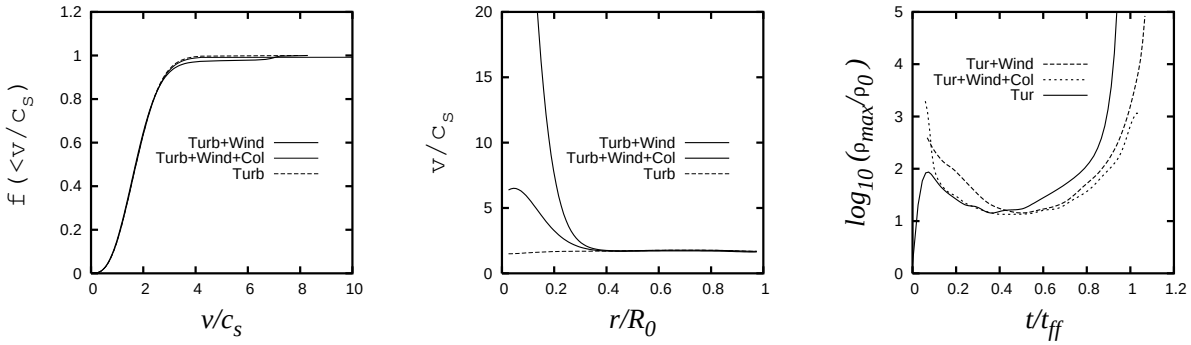

Fig. 2. (left) the velocity distribution of the particles; (middle) the velocity radial profile and (right) the peak density time evolution.

5.2 The effects of winds in the evolution of the turbulent clump.

As one can see in the two first panels of Fig. 2, a very small fraction of gas particles can attain velocities much higher than those velocities provided from the turbulence alone, which are around 2 Mach. Eighty per cent of the simulation particles have velocities less than $v/cs < 4$.

The winds are suddenly activated at the time $t/t_{ff} = 0.05$, when the clump has already acquired a fully flocculent aspect, which is a consequence of the huge number of gas collisions produced randomly across the clump. This time also marks the occurrence of the highest peak in the clump's density curve, shown in the third panel of Fig.2

Besides, we notice by looking at the third panel Fig. 2, that the global collapse of the clump does not change even when the winds are introduced, as the peak density curve of each run goes to higher values. However, the wind of the first kind makes the collapse take place slower as its density peak curve shows less steepness in the middle stages of its evolution.

The iso-density plots for the simulation $Tur+Wind$ are shown in Fig. 3. By the time $t/t_{ff} = 0.36$, we see a void created in the central region of the clump because both the wind particles and those particles which are swept out move towards the outer parts of the clump. However, gravity and viscosity act together in such a way that the particles quickly fill the void, as can be seen in the last panel of Fig. 3.

When we consider the model $Tur + Wind + Col$, so that a collimated gas of particles is ejected, we see that the effects on the clump are more significant, but essentially the same phenomena as seen in the model $Tur + Wind$ take place, as can be seen in Fig. 4.

In Fig.5 we present $3d$ plots of the densest particles for both models. In Figs.6 and 7 we present $3d$ plots at two different times in which one can distinguish the wind and the gas particles.

We emphasize that the fraction of gas swept out by the winds is really significant: hundreds of solar masses move even far beyond the clump radius R_0. In the fourth column of Table 1, we show that the initial mass contained within the radius R_s(which defines the outer boundary of the initial wind configuration) is around 7 and 5 $M_\odot$, respectively. It is then surprising to notice that the total mass dragged outside R_0 by the end of the simulation time is around 359 and 422 $M_\odot$, respectively, as is shown in the fifth column of Table 1.

Lastly, in columns 6 and 7 of Table 1, we show the velocities attained by those particles located far outside the initial clump. Furthermore, we mention that these velocities are not terminal, but are only the velocities during the time we follow these simulations.

6 Discussion

We mentioned in Sect. 3.4 that the clump under consideration here is initially given a ratios of thermal (α) and kinetic energies (β) to the gravitational energy, respectively, such that the clump collapse is greatly favored. In fact, as we see in Sect.5.1, the clump presents a strong collapse towards the central region, in which no fragmentation is observed. This behavior can be seen in other turbulent simulations, when the turbulent Jeans mass (in analogy to the thermal Jeans mass) is large, so that only one turbulent Jeans mass is "contained" in the total clump mass, see Ref.[21].

The winds are activated in a very early stage of the clump evolution, when turbulence is still ongoing. Soon after, turbulence quickly decays, so that a purely gravity driven collapse will take place in the clump. As we see in Sect.5.2, the winds act firstly as a disruptive perturbation on the clump's near environment. Despite of this, the clump particles quickly reform this evacuated central region. Now, in Ref.[22] we found that the wind models show a strong tendency to form accretion centers in the central region of the clump. It was noticed there that great differences appeared when we compared the number and location of the accretion centers obtained for the turbulent clump and for the clump in the presence of wind. Unfortunately, these results are not included in this paper for a lack of space. Although we try to indicate them by means of the first panel of Fig.5.

Thus, in view of these results, we consider that the expected fate of the turbulent clump is really affected by the wind-clump interaction, as compared with the purely gravity driven collapse, despite that it seems to be the dominant physics in determining the time evolution of the clump. This behavior appears to be the case in general, at least for observed gas structures around 0.1 pc in size, as is discussed in Ref.[21].

It must be noted that in this paper, as a first approximation, the wind emission is a unique event, as it is emitted just for only one time. It would be interesting to make that the winds be created

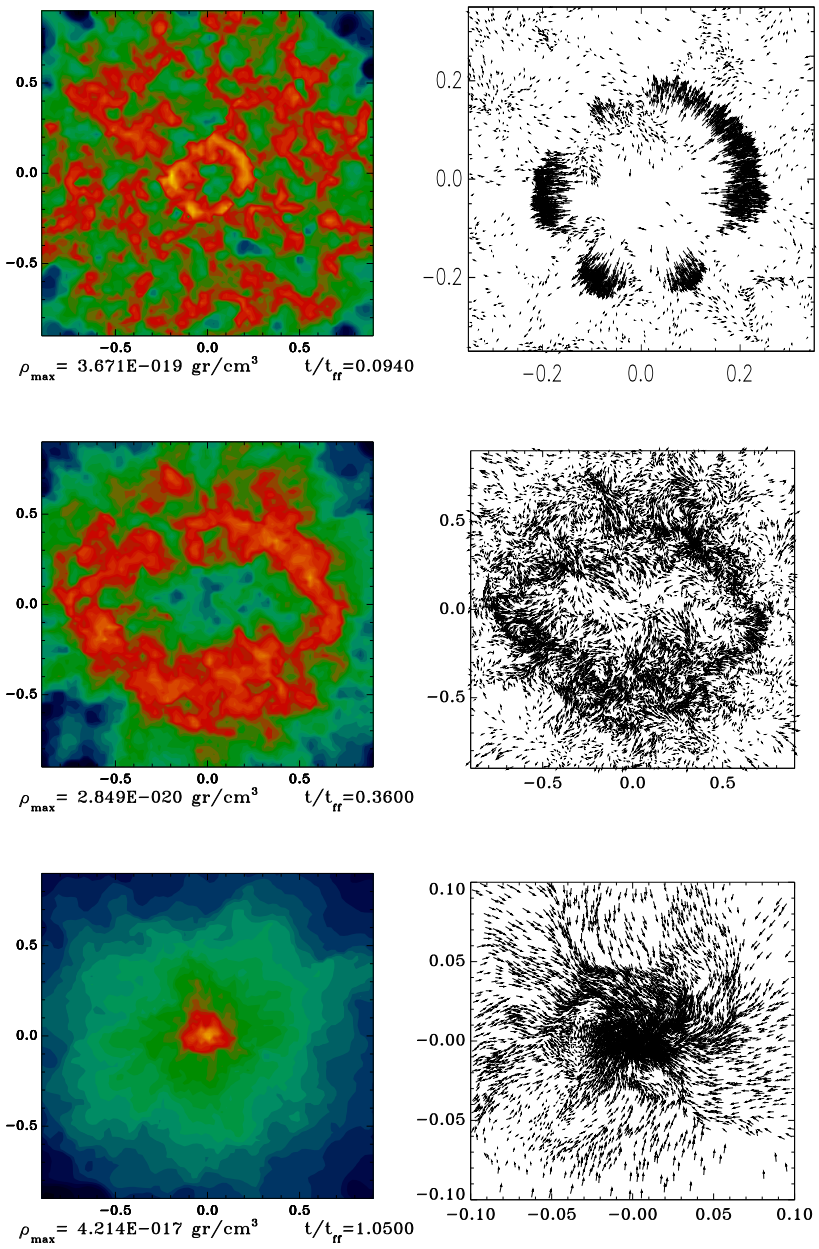

Fig. 3. Iso-density and velocity plots for the model "Tur+Wind".

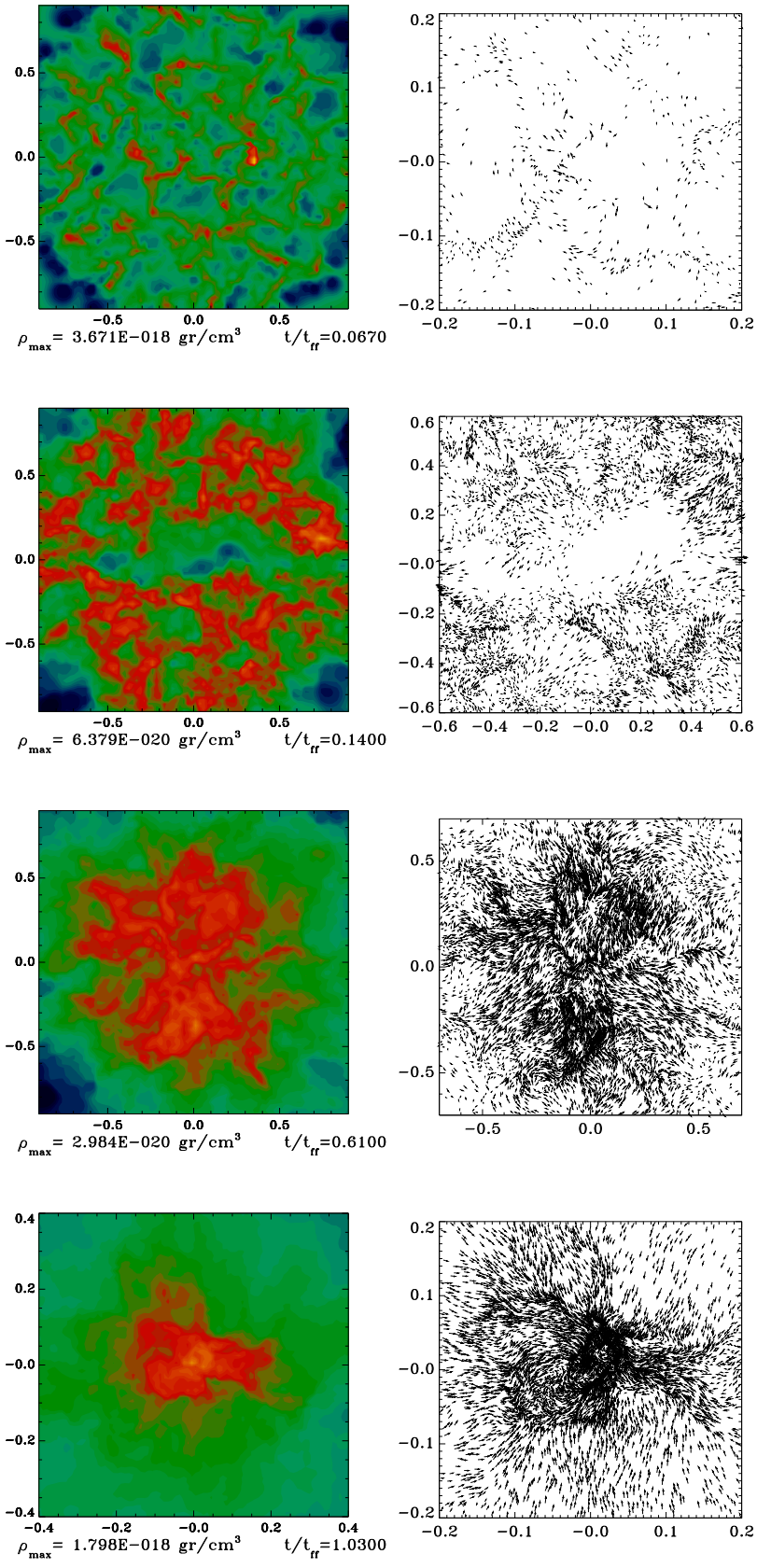
ρ_{max}= 3.671E−018 gr/cm^3 t/t$_{ff}$=0.0670
ρ_{max}= 6.379E−020 gr/cm^3 t/t$_{ff}$=0.1400
ρ_{max}= 2.984E−020 gr/cm^3 t/t$_{ff}$=0.6100
ρ_{max}= 1.798E−018 gr/cm^3 t/t$_{ff}$=1.0300

Fig. 4. Iso-density and velocity plots for the model "Tur+Wind+Col".

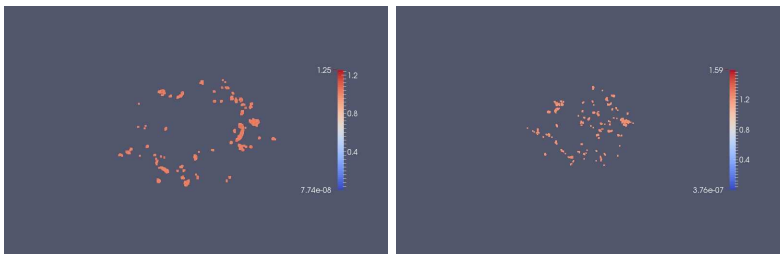

Fig. 5. $3D$ plot of the densest particles for models (left) $Tur + Win$ and (right) $Tur + Win + Col$ at the corresponding snapshots shown in the second lines of Figs. 3 and 4, respectively.

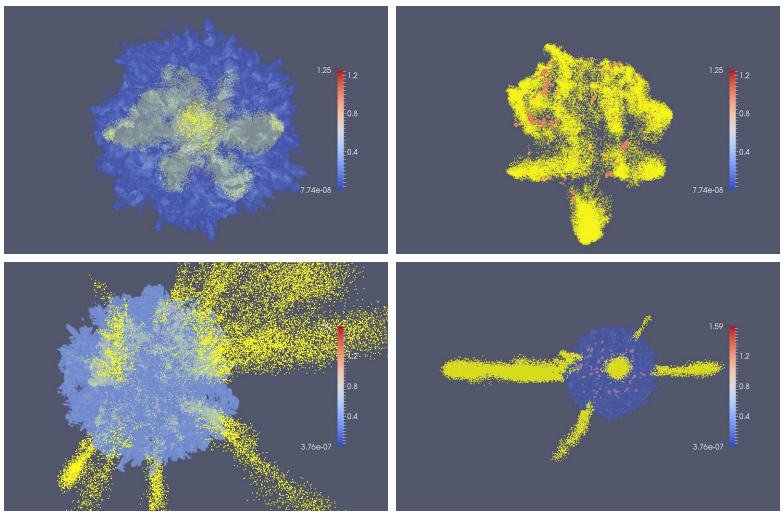

Fig. 6. $3D$ plot of the turbulent clump (in blue) with winds (in yellow) and formed accretion centers (in red) for models (top) $Tur + Win$ and (bottom) $Tur + Win + Col$, corresponding to the plots shown in the second line of Figs.3 and 4, respectively.

and emitted in each time step, so that a continuous emission rate can be simulated. In this case, one would expect that the collapse delay be larger and that the disruption wind effects be more important too.

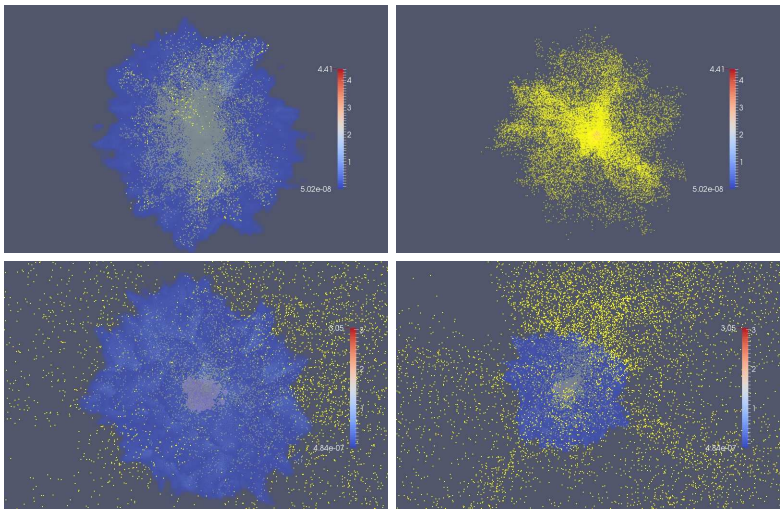

Fig. 7. $3D$ plot of the turbulent clump (in blue) with winds (in yellow) for models (top) $Tur + Win$ and (bottom) $Tur + Win + Col$, corresponding to last snapshot available.

7 Concluding Remarks

A star formation scenario based only on the collapse of turbulence gas structures gives a very highly efficient transformation of the gas into protostars. This points is in contradiction with observations. Besides, a physical system showing simultaneously in-fall and outflow motions are observed in cluster like NGC 1333 and NGC 2264, see Refs.[19] and [20],

Because of this, another scenario must be considered, or at least a theoretical complement to the turbulent model is needed. As we have shown in this paper, the winds must be considered as an additional ingredient to complement the turbulent model with the hope that this new model can alleviate some of the problems mentioned above as they make a delay in the runaway collapse of the clump, see Fig. 2.

We have shown here that all the wind models show a strong tendency to form accretion centers in the central region of the clump. It must be noted that some differences appear when we compare the accretion centers obtained for the wind models, as can be seen in Fig. 5, 6 and 7.

Acknowledgments. We would like to thank ACARUS-UNISON for the use of their computing facilities in the preparation of this paper.

References

1. Bergin, E. and Tafalla, M., 2007, Annu. Rev. Astro. Astrophys. **45**, pp.339-396.
2. Arreaga-García, G., Klapp-Escribano, J. and Gómez-Ramírez,2010, A& A. **509**, pp.A96.
3. Dale, J.E., Bonnell, I.A. and Whitworth, A.P, 2007, MNRAS, **375**, pp. 1291-1298.
4. Li, Z.T. and Nakamura, F., 2006, ApJ, **640**, pp. L187-L190.
5. Nakamura, F. and Li, Zhi-Y, 2007, ApJ, **662**,pp.395-412.
6. Bodenheimer, P., Burkert, A., Klein, R. I. and Boss, A. P. 2000, in Protostars and Planets IV, ed. V. G. Mannings, A. P. Boss and S. S. Russell (Tucson: University of Arizona Press), pp.675-693.
7. Smith, N., 2014, Annual Review of Astronomy and Astrophysics, **52**, pp. 1-45.
8. Gueth, F and Guilloteau, S., 1999, Astron. and Astrophys., **343**, pp.571-584.
9. Dubinski, J., Narayan, R. and Phillips, T.G., 1995, ApJ, **448**, pp. 226-231.
10. Dobbs, C.L., Bonnell, I.A. and Clark, P.C, 2005, MNRAS, **360**, pp. 2-8.
11. Truelove, J.K., Klein, R.I., McKee, C.F., Holliman, J.H., Howell, L.H., and Greenough, J.A., 1997, ApJ, **489**, L179.
12. Bate, M.R. and Burkert, A., 1997, MNRAS, **288**, pp.1060-1072.
13. Boss, A. P., Fisher, R. T., Klein, R., and McKee, C. F. 2000, ApJ, **528**, pp.325-335.
14. Arreaga, G., Klapp, J., Sigalotti, L. and Gabbasov, R. 2007, ApJ, **666**, pp.290-308.
15. Springel, V. 2005, MNRAS, **364**, pp.1105-1134.
16. Monaghan, J. J. and Gingold, R. A. 1983, MNRAS, **204**, pp.715-733.
17. Balsara, D. S. 1995, J. Comput. Phys., **121**, pp.357-372.
18. Hopkins, P.F., 2013, MNRAS, **428**, pp. 2840-2856.
19. Walsh, A.J., Bourke, T.L. and Myers, P. C. 2006, ApJ, **637**, pp.860-868.
20. Peretto, N., André, P. and Belloche, A., 2006, A&A, **445**, pp.979-998.
21. Palau, A., Ballesteros-Paredes, J., Vazquez-Semanedi, E., Sanchez-Monge, A., Estalella, R., Fall, M., Zapata, L.A., Camacho, V., Gomez, L., Naranjo-Romero, R., Busquet, G. and Fontani, F., 2015, MNRAS, **453**, pp.3785-3797.
22. Arreaga-Garcia, G. and Saucedo-Morales, J.C., 2015, Advances in Astronomy, **Vol. 2015**, Art.ID. 196304.